

Testing Gamma-Ray Burst Jet Structure with the Distribution of Gamma-Ray Energy Release

L. Xu, X. F. Wu, and Z. G. Dai

Department of Astronomy, Nanjing University, Nanjing 210093, China

ABSTRACT

We present a general method for testing gamma-ray burst (GRB) jet structure and carry out a comprehensive analysis about the prevalent jet structure models. According to the jet angular energy distribution, we can not only derive the expected distribution of the GRB isotropic-equivalent energy release for any possible jet structure, but also obtain a two-dimensional distribution including redshift z . By using the Kolmogorov-Smirnov test we compare the predicted distribution with the observed sample, and find that the power-law structured jet model is most consistent with the current sample and that the uniform jet model is also plausible. However, this conclusion is tentative because of the small size and the inhomogeneity of this sample. Future observations (e.g., *Swift*) will provide a larger and less biased sample for us to make a robust conclusion by using the procedure proposed in this paper.

Subject headings: gamma rays: bursts — gamma rays: observations — ISM: jets and outflows — methods: statistical

1. INTRODUCTION

Growing evidence such as the achromatic breaks in afterglow light curves of ~ 20 gamma-ray bursts (GRBs) and the observation of polarized emission (Covino et al. 1999; Wijers et al. 1999) suggests that GRBs are produced by collimated jets. Numerous models for the jet configuration have been proposed due to its importance in understanding the burst progenitor and GRB event rates. One leading model is the uniform jet one (e.g., Rhoads 1997; Sari, Piran, & Halpern 1999; Frail et al. 2001; Dai & Cheng 2001), in which the angular energy distribution within the jet is uniform while the nearly constant total energy is collimated into different opening angles. Another is the structured jet model, in which the jet energy and structure are approximately identical for all GRBs, but the energy per solid angle $\epsilon(\theta)$ varies as a function of angle from the jet axis within the structured jet

(Mészáros, Rees, & Wijers 1998; Dai & Gou 2001; Rossi, Lazzati, & Rees 2002; Zhang & Mészáros 2002). Furthermore, although the specific distribution of jet opening angles in the uniform jet model is uncertain, several kinds of distribution such as the power-law, Gaussian and exponential function have been suggested. In this paper we discuss these possible models specifically.

Since a few leading models of jet structure can all explain the observed achromatic breaks in afterglow light curves, some authors attempted to test the geometrical configuration by using other observations. For example, the jet structure could be constrained by considering the luminosity function (e.g., Firmani et al. 2004; Lloyd-Ronning, Dai, & Zhang 2004; Guetta, Piran, & Waxman 2005). The $\log N - \log P$ plot was also used to constrain the jet opening angle distribution for the uniform jet and the star forming rate (Lin et al. 2004; Guetta, Piran, & Waxman 2005). Perna, Sari, & Frail (2003) predicted the observed one-dimensional (1D) distribution of viewing angles, $n(\theta) = dn/d\theta$, in the power-law structured jet model. They found that the predicted distribution could fit the current sample of 16 bursts with modelled angles and known redshifts. Considering the same model, Nakar, Granot, & Guetta (2004) carried out an analysis about the two-dimensional (2D) distribution $n(z, \theta) = d^2n/dz d\theta$. However, they found that the 2D prediction shows a very poor agreement with the same sample, and the hypothesis that the data are drawn from this model is rejected at the 99% confidence level by a 2D Kolmogorov-Smirnov (K-S) test. Based on the standard energy reservoir of GRB jets and the relationship between the cosmic rest frame GRB spectral peak energy and the isotropic gamma-ray energy, i.e., $E_{\text{peak}} \propto E_{\text{iso}}^{1/2}$, Liang, Wu, & Dai (2004) simulated a sample including 10^6 GRBs to test the GRB probability distribution as a function of viewing angle and redshift, and supported the power-law structured jet model. Dai & Zhang (2005) summarized the above tests and performed a global test on the quasi-universal Gaussian-like structured jet. Together with their previous tests with the observed jet break angle vs. isotropic energy ($E_{\text{iso}} - \theta_j$) and observed peak energy vs. fluence relations ($E_{\text{peak}}^{\text{obs}}$ vs. fluence), Zhang et al. (2004) concluded that the current GRB data are generally consistent with the Gaussian-like jet model. These tests can only tentatively support certain possible configuration of the GRB jet, partly because the size of the sample use in the test is too small (but see Cui, Liang, & Lu 2005, who recently adopted the BATSE sample). In this paper, we propose a new method to test the GRB jet structure by using the sample of bursts with measured fluences and redshifts. By considering three jet structure models, i.e., the power-law structured jet model, the Gaussian structured jet model, and the uniform jet model, we work out the theoretical distribution of burst isotropic-equivalent energy release in both 1D distribution $\dot{N}(E) = dN/dE$ and 2D distribution $\dot{N}(E, z) = d^2N/dEdz$ (hereafter, we use E instead of E_{iso} for brevity), and compare them with the observed distribution of E derived from the sample with measured

fluences and redshifts.

This paper is organized as follows: In §2.1 we present several prevalent models for jet structure and the probability distribution of the isotropic-equivalent energy under these models, while in §2.2 we describe our methodology in detail. In §3 we discuss what each model predicts for the observed distribution (in 1D and 2D) of GRB isotropic-equivalent energy release and assess how our numerical results are compared with the current sample by using K-S test. We summarize our results and draw our main conclusions in §4.

2. THEORY

2.1. Models for jet structure

Since the energy release in an explosion plays an important role in determining the progenitors of GRBs and the physics of their central engine, some authors have carried out plenty of analyses about the gamma-ray energy release distribution. Within the uniform jet model, Frail et al. (2001) found that the gamma-ray energy release after beaming correction is narrowly clustered around 5×10^{50} ergs by fitting a sample of 16 well observed GRBs. Using a larger sample, Bloom, Frail, & Kulkarni (2003) obtained a similar result that the gamma-ray energies are well clustered around a median value of 1.33×10^{51} ergs. The gamma-ray energy release should become larger if the gamma-ray radiation efficiency is considered (Xu & Dai 2004). Panaitescu & Kumar (2001, 2002) modelled the broadband emission of several GRB afterglows and obtained a similar value of the kinetic energy. Furthermore, Wu, Dai, & Liang (2004) derived a jet break time-flux density relationship and constrained some physical parameters of gamma-ray burst afterglows. The jet break relation supports the “standard candle” hypothesis of the afterglows by an entirely different approach. We therefore adopt a standard value for GRB jet energy $E_j = 10^{51}$ ergs throughout this paper. According to the presently measured isotropic-equivalent energy, we adopt the upper limit of the isotropic-equivalent energy as $E_{\max} = 10^{55}$ ergs.

According to the angular energy distribution for any plausible jet model, one can obtain the isotropic-equivalent energy as a function of θ . The isotropic-equivalent energy, E , is defined as $E(\theta) = 4\pi\epsilon(\theta)$, where θ is the angle from the jet axis and $\epsilon(\theta)$ is the energy per solid angle.

In the power-law structured jet (PLSJ) model, all GRBs are supposed to have a similar jet profile, and their different observed properties are due to different observer’s viewing angles. Under the power-law jet scenario, the angular distribution of the isotropic-equivalent

energy is

$$E(\theta) = \frac{E_c}{[1 + (\theta/\theta_c)^{k_E l_E}]^{1/l_E}}, \quad (0 \leq \theta \leq \pi/2), \quad (1)$$

where l_E determines the sharpness of the transition from the core to wing, and k_E represents the profile of the jet wing. The opening angle of the core θ_c is introduced to avoid the divergence of the total energy. E_c is defined as $E_c = E(0)$, and equals to the maximum isotropic-equivalent energy E_{\max} . Below we assume $l_E = +\infty$ for simplicity. If all bursts were observable, then in a structured jet model, the probability for a viewing angle θ is $P(\theta)d\theta \approx \theta d\theta$. From the relation $P(\theta)d\theta = P(E)dE$, we obtain the normalized probability density at a given isotropic-equivalent energy E ,

$$P(E) \approx \frac{8}{\pi^2} \frac{\theta_c^2}{k_E E_c} \left(\frac{E_c}{E} \right)^{1+2/k_E}, \quad ((2\theta_c/\pi)^{k_E} E_c \leq E \leq E_c). \quad (2)$$

In the Gaussian structured jet (GSJ) model, the isotropic-equivalent energy distribution that varies with the angle from the jet axis is (Zhang & Mészáros 2002)

$$E(\theta) = E_c e^{-\frac{\theta^2}{2\theta_c^2}}, \quad (0 \leq \theta \leq \pi/2), \quad (3)$$

where $E_c = E(0)$, and θ_c is the characteristic jet angular width. According to the same derivation as in the power-law structured jet model, we have the normalized probability at a given isotropic-equivalent energy E ,

$$P(E) = \frac{8}{\pi^2} \frac{\theta_c^2}{E_c}, \quad (E_c e^{-\pi^2/8\theta_c^2} \leq E \leq E_c). \quad (4)$$

Similarly we assume $E_c = 10^{55}$ ergs.

In the uniform jet (UJ) model (e.g., Lamb, Donaghy, & Graziani 2005), all GRBs produce jets with different jet opening angles θ_j . The structure of a uniform jet reads

$$E(\theta) = \begin{cases} E, & 0 \leq \theta \leq \theta_j, \\ 0, & \theta_j < \theta \leq \pi/2. \end{cases} \quad (5)$$

Assuming $f(E)$ is the probability that a GRB releases the isotropic energy between E and $E + dE$, the probability that we observe a specified E is given by $P(E) = f(E)(1 - \cos \theta_j)$. Using the Frail's relation, $E_j = E(1 - \cos \theta_j) \approx \text{constant}$, we obtain the probability distribution of the isotropic energy

$$P(E) \approx f(E) \frac{E_j}{E}, \quad (E_j \leq E \leq E_{\max}), \quad (6)$$

Next we turn to discuss the specified form of $f(E)$. As for the GRB opening angle distribution, Lin et al. (2004) studied three cases in which the GRB opening angle θ_j follows a power-law, exponential, or Gaussian distribution. Here we also consider these three cases. We assume that the first probability distribution of isotropic-equivalent energy follows a power-law function with index ζ ,

$$f(E) = \frac{1 + \zeta}{E_{\max}^{1+\zeta} - E_j^{1+\zeta}} E^\zeta, \quad (E_j \leq E \leq E_{\max}). \quad (7)$$

It is worth noting that $f(E)$ should be normalized, i.e. $\int_{E_j}^{E_{\max}} f(E) dE = 1$. The second probability distribution for $f(E)$ is an exponential function with parameter λ ,

$$f(E) = \frac{\lambda e^{\lambda E_j}}{1 - e^{-\lambda(E_{\max} - E_j)}} e^{-\lambda E}, \quad (E_j \leq E \leq E_{\max}), \quad (8)$$

which has also been normalized. Finally, if $f(E)$ is a Gaussian distribution with the mean energy \bar{E} and standard scatter σ , we have

$$f(E) = \frac{a}{\sqrt{2\pi}\sigma} e^{-\frac{(E - \bar{E})^2}{2\sigma^2}}, \quad (E_j \leq E \leq E_{\max}), \quad (9)$$

where a is the normalization factor satisfying $\int_{E_j}^{E_{\max}} f(E) dE = 1$.

2.2. Detections

For a power-law photon spectrum, the photon luminosity in the triggering band $\nu_l - \nu_u$ is given by

$$L_{\text{ph},[\nu_l, \nu_u]} = \frac{E}{Th\nu_l} \frac{\alpha - 2}{\alpha - 1} \left(\frac{\nu_l}{\nu_1} \right)^{2-\alpha} \frac{1 - (\nu_u/\nu_l)^{1-\alpha}}{1 - (\nu_2/\nu_1)^{2-\alpha}}, \quad (10)$$

where α is the photon spectrum index, and ν_l and ν_u are the lower and upper limiting frequencies of a GRB detector respectively. For the BATSE triggering channel, $\nu_l = 50$ keV and $\nu_u = 300$ keV. The E is the isotropic-equivalent γ -ray energy in a range of $\nu_1 = 0.1$ keV to $\nu_2 = 10^4$ keV at the GRB's cosmological rest frame. The mean spectral peak energy for GRBs is $\langle E_p \rangle \sim 250$ keV (Preece et al. 2000). According to the spectral fit, we take $\alpha \approx 1$ for the frequency range $\nu_l < \nu < \nu_u$ in the following calculations (Band et al. 1993). Then the photon luminosity can be simplified as

$$L_{\text{ph},[\nu_l, \nu_u]} = \frac{E}{Th(\nu_2 - \nu_1)} \ln \left(\frac{\nu_u}{\nu_l} \right), \quad (11)$$

where T is an “effective” duration that the burst would have if its energy output is constant at the peak value rather than the highly variable one.

The detector can be triggered if the photon flux is greater than the limiting photon flux that is determined by the threshold of the GRB detector. Thus we can determine the maximum redshift z_{\max} of the burst through

$$\frac{L_{\text{ph},[\nu_l, \nu_u]}(E, T)}{4\pi D^2(z_{\max})(1 + z_{\max})^\alpha} = F_{\text{ph,lim}}, \quad (12)$$

where $D(z)$ is the comoving distance of the source to the observer and $F_{\text{ph,lim}}$ is the triggering threshold of the detector.

The observed burst rate with isotropic-equivalent energy between E and $E + dE$ is given by

$$\frac{d^2 N(E)}{dt_{\text{obs}} dE} = P(E) \int_0^{z_{\max}(E, T)} \frac{R_{\text{GRB}}}{1 + z} \frac{dV}{dz} dz, \quad (13)$$

where R_{GRB} is the GRB rate per unit comoving volume per unit comoving time, and $V(z)$ is the comoving volume. In a flat cosmology $dV(z)/dz = 4\pi D^2(z) dD(z)/dz$.

Nakar et al. (2004) used the flux table of the BATSE 4B Catalog and Band spectrum to estimate the distribution of T . They found a lognormal distribution,

$$\frac{d\bar{P}}{d \ln T} = T \bar{P}(T) = \frac{1}{\sigma_{\ln T} \sqrt{2\pi}} \exp \left[-\frac{(\ln T - \mu)^2}{2\sigma_{\ln T}^2} \right], \quad (14)$$

where $\mu = 2.15$ and $\sigma_{\ln T} = 0.87$ ($T = 8.6_{-5}^{+12}$ s).

Next, we consider the selection effect in redshift identification. Bloom (2003) found that there are strong observational biases in ground-based redshift discovery, and suggested to use a probability function related to the luminosity distance to minimize this effect. $P_L(z)$ is constructed:

$$P_L(z) = \begin{cases} 1, & z \leq z_l, \\ \left(\frac{D_L(z)}{D_L(z_l)} \right)^L, & z > z_l. \end{cases} \quad (15)$$

Via K-S test, Bloom constrained $z_l < 1.25$ and $-3 < L < -1$. We here adopt the value of $z_l = 1$ and allow the parameter L to vary between -3 and -1 case-by-case in order to get a better fit. Using the distribution of T and taking into account the redshift selection effect, we generalize the distribution of isotropic-equivalent jet energy as

$$\dot{N}(E) = \frac{d^2 N(E)}{dt_{\text{obs}} dE} = P(E) \int_0^{+\infty} \bar{P}(T) dT \int_0^{z_{\max}(E, T)} P_L(z) \frac{R_{\text{GRB}}}{1 + z} \frac{dV}{dz} dz. \quad (16)$$

Furthermore, since in the 1D analysis the integration over redshift hides certain important information about the distribution as a function of z , we extend the 1D distribution $\dot{N}(E)$ to the 2D distribution $\dot{N}(E, z)$,

$$\dot{N}(E, z) = \frac{d^3 N(E)}{dt_{\text{obs}} dE dz} = P(E) \left(\int_0^{T_{\text{max}}(E, z)} \bar{P}(T) dT \right) P_L(z) \frac{R_{\text{GRB}}}{1+z} \frac{dV}{dz}, \quad (17)$$

where $T_{\text{max}}(E, z)$ is determined by equation (12).

Finally, we consider the GRB event rate. It has been suggested that GRBs follow the star formation rate, because GRBs are probably produced in the final gravitational collapse of massive stars (e.g. Woosley 1993; Paczynski 1998). Here we assume that the rate of GRBs traces the global star formation history of the universe, $R_{\text{GRB}}(z) \propto R_{\text{SF}}(z) \propto R_{\text{SN}}(z)$. Following Porciani & Madau (2001), we employed three different kinds of global star formation rate (SFR) model. These three SFR models are similar at $z < 1$. The main difference is at high redshifts: in model 1, the SFR decreases at $z > 1.5$; in model 2, the SFR contains the dust extinction effect and remains constant at $z > 2$; and in model 3, the SFR increase at high redshifts after a correction due to a large amount of dust extinction. These SFR models are all in an Einstein-de Sitter universe with parameter $\Omega_M = 1.0$, $\Omega_K = 0.0$, $\Omega_\Lambda = 0.0$, and $H_0 = 65 \text{ km s}^{-1} \text{ Mpc}^{-1}$. We can obtain the SFR in any cosmology with parameters Ω_M , Ω_Λ , Ω_K and H_0 through the formulation in the appendix of Porciani & Madau (2001).

We assume that all stars with masses $M > 30M_\odot$ explode as Type Ib/Ic SNe, and adopt the initial mass function suggested by Madau & Pozzetti (2000). The SN Ib/Ic rate can then be estimated by $R_{\text{SN Ib/c}} = f_{\text{SN Ib/c}} R_{\text{SF}} = 1.8 \times 10^{-3} M_\odot^{-1} R_{\text{SF}}$. Lamb (1999) showed that the observed ratio of the rate of GRBs to the rate of Type Ib/Ic SNe in the observable universe is $R_{\text{GRB}}/R_{\text{Type Ib/c}} \sim 10^{-5}$. Therefore the GRB event rate can be approximated by $R_{\text{GRB}} = f_{\text{GRB}} R_{\text{SF}} = 10^{-8} M_\odot^{-1} R_{\text{SF}}$.

3. Results

In order to test the configuration of jets, we firstly perform a theoretical analysis in two limits: the rate of GRBs at low and high values of isotropic-equivalent energy. The analysis can also predict and test our numerical results. Secondly, we present detailed results of numerical calculations, which are well consistent with the theoretical one.

We used the same parameters as in Perna et al. (2003) and Nakar et al. (2004). The triggering threshold is $F_{\text{ph,lim}} = 0.424 \text{ photons cm}^{-2} \text{ s}^{-1}$, and the cosmological parameters

are: $\Omega_M = 0.3$, $\Omega_\Lambda = 0.7$, and $H_0 = 71 \text{ km s}^{-1} \text{ Mpc}^{-1}$.

3.1. Theoretical analysis

The comoving distance in the currently adopted cosmology can be approximated by (Wu, Dai, & Liang 2004)

$$D(z) \simeq \frac{c}{H_0} \frac{z}{1 + 0.29z}. \quad (18)$$

Combined with equation (12), the photon flux in both limits reads

$$F_{\text{ph,lim}} \approx 0.55 \text{ photons} \cdot \text{cm}^{-2} \cdot \text{s}^{-1} E_{53} \left(\frac{T}{8 \text{ s}} \right)^{-1} \times \begin{cases} z_{\text{max}}^{-2}, & z_{\text{max}} < 1, \\ 0.29^2 z_{\text{max}}^{-1}, & z_{\text{max}} > 4. \end{cases} \quad (19)$$

We take the conventional notation $Q = Q_x \cdot 10^x$. For a given triggering instrument, $F_{\text{ph,lim}}$ is known. Therefore in the limit of $z_{\text{max}} < 1$ the maximum redshift that a GRB can be detected is

$$z_{\text{max}} = 1.15 \left(\frac{F_{\text{ph,lim}}}{F_{\text{ph,lim}}^{\text{BATSE}}} \right)^{-1/2} E_{53}^{1/2} \left(\frac{T}{8 \text{ s}} \right)^{-1/2}, \quad (20)$$

while in the limit of $z_{\text{max}} > 4$, it follows

$$z_{\text{max}} = 0.11 \left(\frac{F_{\text{ph,lim}}}{F_{\text{ph,lim}}^{\text{BATSE}}} \right)^{-1} E_{53} \left(\frac{T}{8 \text{ s}} \right)^{-1}. \quad (21)$$

Here we scale the detection threshold to that of the BATSE triggering channel. Assuming an empirical $T \sim 8 \text{ s}$, the maximum redshift is $z \propto E^{1/2}$ for low energies $E < 10^{53} \text{ ergs}$, and $z \propto E$ for extremely large energies $E > 10^{54} \text{ ergs}$. In the following analysis, we take the star formation rate model 2 as an example.

In the case of $z_{\text{max}} < 1$, i.e., for GRBs with low isotropic energy of $E < 10^{53} \text{ ergs}$, the integration over redshift z in equation (13) gives $43h_{65}f_{\text{GRB},-8}(F_{\text{ph,lim}}/F_{\text{ph,lim}}^{\text{BATSE}})^{-3/2}E_{53}^{3/2}(T/8 \text{ s})^{-3/2} \text{ yr}^{-1}$, where $h_{65} = H_0/65 \text{ km} \cdot \text{s}^{-1} \cdot \text{Mpc}^{-1}$. The differential rate of bursts for the power-law structured jet model is

$$\frac{d^2 N(E)}{dt_{\text{obs}} d\log_{10} E} \simeq 0.4h_{65} \left(\frac{k_E}{2.0} \right)^{-1} \left(\frac{\theta_c}{0.01} \right)^2 E_{c,55}^{2/k_E} f_{\text{GRB},-8} \left(\frac{F_{\text{ph,lim}}}{F_{\text{ph,lim}}^{\text{BATSE}}} \right)^{-3/2} \left(\frac{T}{8 \text{ s}} \right)^{-3/2} E_{53}^{1/2} \text{ yr}^{-1}. \quad (22)$$

Similarly the differential rate for the Gaussian structured jet model is

$$\frac{d^2 N(E)}{dt_{\text{obs}} d\log_{10} E} \simeq 0.2h_{65} \left(\frac{\theta_c}{0.05} \right)^2 f_{\text{GRB},-8} \left(\frac{F_{\text{ph,lim}}}{F_{\text{ph,lim}}^{\text{BATSE}}} \right)^{-3/2} \left(\frac{T}{8 \text{ s}} \right)^{-3/2} E_{53}^{3/2} \text{ yr}^{-1}. \quad (23)$$

For the uniform jet model, we just present the rate in the case that the distribution of isotropic-equivalent energy is an exponential function,

$$\frac{d^2 N(E)}{dt_{\text{obs}} d\log_{10} E} \simeq 14 h_{65}^4 \lambda_{-53} E_{j,51}^{1/2} (e^{0.01 \lambda_{-53} E_{j,51}}) f_{\text{GRB},-8} \left(\frac{F_{\text{ph,lim}}}{F_{\text{ph,lim}}^{\text{BATSE}}} \right)^{-3/2} \left(\frac{T}{8 \text{ s}} \right)^{-3/2} E_{53}^2 e^{-\lambda_{-53} E_{53}} \text{ yr}^{-1}, \quad (24)$$

where $\lambda = 10^{-53} \lambda_{-53} \text{ erg}^{-1}$ and $E_{j,51}$ is the jet energy in units of 10^{51} ergs.

In the case of $z_{\text{max}} > 4$, i.e., $E > 10^{54}$ ergs, the integration over redshift z in equation (13) gives $\sim 1.86 \times 10^3 h_{65}^4 f_{\text{GRB},-8} g(z_{\text{max}}) \text{ yr}^{-1}$. The value of $g(z_{\text{max}})$ ranges from 0.03 to 0.28. To obtain an estimation, we adopt $g(z_{\text{max}}) \approx 0.1$. Then the differential GRB rate for the power-law structured jet model is

$$\frac{d^2 N(E)}{dt_{\text{obs}} d\log_{10} E} \simeq 1.7 h_{65}^4 \left(\frac{k_E}{2.0} \right)^{-1} \left(\frac{\theta_c}{0.01} \right)^2 E_{c,55}^{2/k_E} f_{\text{GRB},-8} \frac{g(z_{\text{max}})}{0.1} E_{53}^{-1} \text{ yr}^{-1}. \quad (25)$$

Similarly, the rate for the Gaussian structured jet model is

$$\frac{d^2 N(E)}{dt_{\text{obs}} d\log_{10} E} \simeq 0.85 h_{65}^4 f_{\text{GRB},-8} \frac{g(z_{\text{max}})}{0.1} \left(\frac{\theta_c}{0.05} \right)^2 \text{ yr}^{-1}. \quad (26)$$

At last, for the uniform jet model, if the distribution of jet isotropic-equivalent energy conforms to an exponential distribution, then the differential burst rate is

$$\frac{d^2 N(E)}{dt_{\text{obs}} d\log_{10} E} \simeq 60.4 h_{65}^4 \lambda_{-53} (e^{0.01 \lambda_{-53} E_{j,51}}) E_{j,51}^{1/2} f_{\text{GRB},-8} \frac{g(z_{\text{max}})}{0.1} E_{53}^{1/2} e^{-\lambda_{-53} E_{53}} \text{ yr}^{-1}. \quad (27)$$

Figure 1 shows differential rates of GRBs determined by equation (13). Different lines correspond to the predicted distributions derived from different possible models. It can be seen that the above analytical expressions describe the rate quite well at low and high limits of E . The predicted GRB rates for these models differ from each other significantly, especially at extremely low and high energy limits. Such evident differences enable us to find the best model for the jet structure, if the sample contains enough bursts. Therefore the 1D comparison between the predicted distribution of E and the observed sample is available, although the integration over redshift conceals much information.

3.2. Numerical analysis

To compare the theoretical distributions derived in §2, we consider a sample of GRBs whose fluences and redshifts are measured. Such a sample including 41 bursts are listed in

Table 1. This table does not contain GRBs such as GRB 980329, 980519, 000630, 020331, 030115 and 040511, because of the large uncertainties of their redshifts. We rule out 2 GRBs in this table: GRB 980425 and 031203, because they form a peculiar subclass characterized by their unusually low isotropic gamma-ray energy releases and other unusual properties. For example, these two GRBs violate the $E_{\gamma,\text{iso}} - E_{\text{peak}}$ relation and the luminosity-spectral lag relation (Sazonov, Lutovinov, & Sunyaev 2004). Furthermore, Yamazaki, Yonetoku and Nakamura (2003) found that the observed unusual properties of the prompt emission of GRB 980425 could be explained by using an off-axis jet model of GRBs, such as the extremely low isotropic equivalent γ -ray energy, the low peak energy, and the high fluence ratio, and the long spectral lag. Ramirez-Ruiz et al. (2004) also argued that the observed data for GRB 031203 are more consistent with a GRB seen at an angle of about twice the opening angle of the central jet. Since we do not consider the off-axis case in our model analysis, we rule out these two GRBs in the numerical analysis. Therefore, we finally have 39 bursts available in our analysis. We have calibrated the isotropic-equivalent energy release in a fixed cosmological bandpass, 0.1 keV-10 MeV, using the cosmological k-correction (Bloom, Frail, & Sari 2001). The calorimetric isotropic-equivalent energy is given by $E = 4\pi D_L^2 S_{[0.1-10^4]} / (1+z)$.

We calculate the 1D distribution $\dot{N}(E)$ under three jet structure scenarios, and perform K-S test to assess the compatibility of the theoretical distributions with the observed data. We describe the significance level for the result of K-S test as $P_{\text{k-s}}$. Small values of $P_{\text{k-s}}$ show that the theoretical distributions and the observed data are significantly different (Press et al. 1997). In the analysis below, we take the star formation rate model 2 and $L = -1.0$ as an example. We also perform the test for other star formation rate models as well as other values of L , and ultimately obtain similar results.

Figure 2 shows that the predicted distribution peaks approximately at the same energy for different SFR models. Three SFR models result in slight differences in the predicted distribution if we adopt other parameters with the same values. In Figure 3 the 2D grey contours show the confidence level (for the null hypothesis that the observed data are drawn from this model) as a function of k_E and θ_c . We find that the predicted distribution is consistent with the observations at the confidence level of $> 40\%$ while the parameters k_E and θ_c are changed in a wide range. For other star formation rate models, the power-law structured jet model also agrees with the observational data reasonably well.

However, the distribution derived from the Gaussian jet model does not agree with the observations even if the parameter θ_c is changed in a wide range. Figure 4 shows the theoretical distribution of GRB isotropic energy for different star formation rate models. The theoretical distribution peaks at higher energy compared with the observed sample. Figure 5 shows the predicted and observed cumulative distributions of GRB isotropic energy for three

different values of L , assuming the star formation rate model 2. Different star formation rate models and different values of L only lead to a slight difference in the distribution. The Gaussian jet model predicts that most GRBs are detected within its central core where the isotropic energy is large and nearly constant. This is because the energy decreases exponentially at the wing and the GRB cannot be triggered by the detectors. However, we note that if we introduce some dispersion on the value of the central angle θ_c , this inconsistency may be reduced (Zhang et al. 2004; Dai & Zhang 2005).

In the uniform jet model, we have considered three cases in which $f(E)$ is a power-law, exponential, or Gaussian function. By comparing the theoretical calculation and the observational data using the K-S test, we obtain a confidence level for the hypothesis that the observational data is drawn from the theoretical distribution. In the case of a power-law distribution, the result of the K-S test depends mainly on the value of the index ζ . Our numerical results show that when ζ varies between -0.99 and -0.79, the theoretical distribution is compatible with the observed data at the confidence level of $> 40\%$. This confidence reaches a maximum of 90% for $\zeta = -0.91$. We show in Figure 6 the predicted and observed distributions of GRB isotropic energy for three different values of ζ . Figure 7 presents the predicted and observed cumulative distributions of GRB isotropic energy for three different values of ζ .

In the case of exponential and Gaussian distributions, the results of the K-S test also depend on the parameters. But the theoretical distributions are consistent with the observations at the confidence level of $< 5\%$, even though the parameters are changed greatly. Figures 8 and 9 show the differential and cumulative distributions of GRB isotropic energy respectively. Despite the variation of the parameter λ , the figures show a poor consistency between the theoretical prediction and the observed data. Figures 10 and 11 exhibit similar results for the case that $f(E)$ follows a Gaussian function.

We next consider the 2D distribution $\dot{N}(E, z)$. The distribution of GRBs is a function of both isotropic equivalent energy and redshift. In the 1D analysis, the information contained in the redshift space is concealed by the integration over redshift. In order to explore the overall information about the distribution of GRBs, we extend the distribution from one dimension to two dimensions, and compare it with the observed sample (see Figs. 12-16). We performed 2D K-S test to check the consistency of the predicted 2D distribution with the observations. For the sample of 39 bursts, a 2D K-S test shows that for the power-law structured jet model, the predicted distribution is consistent with the observations at the confidence level of $> 40\%$ while the parameters k_E and θ_c are changed in a wide range. When adopting the value of parameters $k_E = 2.2$ and $\theta_c = 0.02$, we obtain the best fit, at the confidence level of 58%. For the uniform jet model in the power-law case, the model

with SFR2, $L = -1$, and $\zeta = -0.92$ corresponds to a best fit, at the confidence level of 57%. When ζ varies between -0.97 and -0.85, the predicted distribution is compatible with the observed data at the confidence level of $> 40\%$. In the exponential and Gaussian case, we found that the hypothesis that the data are drawn from these three models is completely rejected. This conclusion is unchanged for different values of the parameters.

However, this conclusion is tentative, because the sample suffers from various observational biases, such as GRB detection, localization, and especially the selection effect in the identification of redshift (Bloom 2003). Nakar et al. (2004) suggested that the selection effect in redshift can be minimized by testing the θ distribution for a given redshift. But the size of the sample is greatly reduced in this method. With the cumulation of the sample in the future, this method might be used to test the configuration of jets in GRBs.

4. Discussion and Conclusion

In this paper, we have worked out the theoretical distribution of burst isotropic-equivalent energy in 1D $\dot{N}(E) = dN/dE$ and in 2D $\dot{N}(E, z) = dN^2/dEdz$ for several jet structure models. The figures and analyses above show that theoretically the GRB rates predicted by different models differ from each other greatly. It is possible for us to find the true model by the method shown here if the sample is large enough. Based on the theoretical analysis in §3.2, we carried out numerical calculations and compared $\dot{N}(E) = dN/dE$ and $\dot{N}(E, z) = dN^2/dEdz$ with the the observed sample of GRBs with known fluences and redshifts. Via K-S test, we found that the power-law structured jet model and the uniform jet model can be consistent with the currently observed data at a confidence level of $\geq 40\%$ under certain circumstances.

One advantage of our work over Perna et al. (2003) and Nakar et al. (2004) lies in the fact that the sample of bursts with measured redshifts and fluences is larger than the one with known redshifts and modelled angles. The sample of bursts with known redshift and modelled angle is too small (currently 16 GRBs). According to the relation $t_j \propto \theta_j^{8/3}$ (Sari et al. 1999), if the jet opening angle θ_j is small, the jet break time t_j probably is so early that there is only the upper limit on it. In the contrary, if θ_j is large, the late-time optical transient may be too dim to be detected. As a result, this selection effect in detecting t_j leads to a small sample of bursts with measured jet break times. However, the sample of bursts with measured fluences and redshifts does not suffer from such selection effect. This larger sample helps us to draw a stronger conclusion.

However, it is worth noting that all results above are obtained under the following

assumptions. First, the isotropic-equivalent energy release in gamma-ray band is assumed to be proportional to the total isotropic-equivalent energy of the bursts. Second, we consider the simplifying assumption that the theoretical model is strictly consistent with the actual jet structure. These theoretical models predict a smooth, broken power-law light curve. However, recent observations revealed variabilities in some afterglow light curves such as in GRB 021004 (Fox et al. 2003). One leading model named “patchy shell” model attributes this fluctuation in light curves to random angular fluctuation of the energy per solid angle (Kumar & Piran 2000; Nakar, Piran, & Granot 2003). In this paper, we consider a regular energy distribution in the jet rather than with some random angular fluctuations. This simplifying assumption may result in an underestimate of the number of energetic events.

Third, the current sample of 39 bursts with measured redshifts suffers from numerous selection effects, especially in optical afterglow detections and redshift identifications. To reduce these effects, we used a strategy suggested by Bloom (2003). On the other hand this method might introduce a systematic error into the result. To reach a robust conclusion, Nakar et al. (2004) put forward an approach to minimize the selection effect in z , i.e., to test the distribution for a given z . In our work, to avoid this selection effect and reduce the dependence on SFR model, we need to derive the distribution of isotropic-equivalent energy for a fixed redshift $\dot{N}(E)|_z$. However, this method requires a large sample of bursts with measured fluences and with the same redshift, while there are only a few bursts are detected with the same redshift. With a larger sample this method shown here can be expected to give a stronger conclusion. With the advent of the *Swift* era, the sample of GRBs with measured fluence and redshift is anticipated to be much larger than the current one. The large sample of bursts detected by the same detector will be having the same parameters such as the detector sensitivity, thus reducing the uncertainty and reaching a stronger conclusion.

We thank E. W. Liang, D. Xu and Z. P. Jin for their helpful discussions. This work was supported by the National Natural Science Foundation of China (grants 10233010 and 10221001) and the Ministry of Science and Technology of China (NKBRSF G19990754).

REFERENCES

- Amati, L., Frontera, F., in 't Zand, J. J. M., et al. 2004, *A&A*, 426, 415
- Amati, L., Frontera, F., Tavani, M., et al. 2002, *A&A*, 390, 81
- Andersen, M. I., Hjorth, J., Pedersen, H., et al. 2000, *A&A*, 364, L54
- Antonelli, L. A., Piro, L., Vietri, M., et al. 2000, *ApJ*, 545, L39
- Atteia, J.-L. 2003, *A&A*, 407, L1
- Band, D. J. et al. 1993, *ApJ*, 413, 281
- Barraud, C. et al. 2003, *A&A*, 400, 1021
- Barth, A. J. et al. 2003, *ApJ*, 584, L47
- Berger, E. et al. 2001, *ApJ*, 556, 556
- Berger, E., Gladders, M., & Oemler, G. 2005, GCN Report 3201
- Berger, E., & Becker, G. 2005, GCN Report 3520
- Bloom, J. S. 2003a, *AJ*, 125, 2865
- Bloom, J. S., Berger, E., Kulkarni, S. R., Djorgovski, S. G., & Frail, D. A. 2003b, *AJ*, 125, 999
- Bloom, J. S., Djorgovski, S. G., & Kulkarni, S. R. 2001a, *ApJ*, 554, 678
- Bloom, J. S., Djorgovski, S. G., Kulkarni, S. R., & Frail, D. A. 1998, *ApJ*, 507, L25
- Bloom, J. S., Frail, D. A., & Kulkarni, S. R. 2003c, *ApJ*, 594, 674
- Bloom, J. S. et al. 1999, *Nature*, 401, 453
- Bloom, J. S., Frail, D. A., & Sari, R. 2001, *AJ*, 121, 2879
- Bloom, J. S., Morrell, N., & Mohanty, S. 2003d, GCN Report 2212
- Castro, S. M., Diercks, A., Djorgovski, S. G., Kulkarni, S. R., Galama, T. J., Bloom, J. S., Harrison, F. A., & Frail, D. A. 2000a, GCN Report 605
- Castro, S. M., Djorgovski, S. G., Kulkarni, S. R., Bloom, J. S., Galama, T. J., Harrison, F. A., & Frail, D. A. 2000b, GCN Report 851

Table 1. Compilation of Spectra and Energetics Input Data

GRB ^a	z	S_γ ^b [10^{-6} erg cm $^{-2}$]	Bandpass [keV]	$[\alpha, \beta]$ ^c	E_p^{obs} ^d [keV]	References ($z, S_\gamma = S, t_{\text{jet}} = t, n, \alpha, \beta, E_p$)
970228	0.6950	11.00	40, 700	-1.54, -2.50	115	$z: 1, S: 2, \alpha: 2, \beta: 2, E_p: 2$
970508	0.8349	1.80	40, 700	-1.71, -2.20	79	$z: 3, S: 2, \alpha: 2, \beta: 2, E_p: 2$
970828	0.9578	96.00	20, 2000	-0.70, -2.07	298	$z: 4, S: 5, \alpha: 6, \beta: 5, E_p: 5$
971214	3.4180	8.80	40, 700	-0.76, -2.70	155	$z: 7, S: 2, \alpha: 2, \beta: 2, E_p: 2$
980326	1.0000	0.75	40, 700	-1.23, -2.48	47	$z: 8, S: 2, \alpha: 2, \beta: 2, E_p: 9$
980425	0.0085	3.87	20, 2000	-1.27, -2.30 *	118	$z: 10, S: 5, \alpha: 5, E_p: 5$
980613	1.0969	1.00	40, 700	-1.43, -2.70	93	$z: 11, S: 2, \alpha: 2, \beta: 2, E_p: 2$
980703	0.9662	22.60	20, 2000	-1.31, -2.40	254	$z: 12, S: 5, \alpha: 6, \beta: 5, E_p: 5$
990123	1.6004	300.00	40, 700	-0.89, -2.45	781	$z: 13, S: 2, \alpha: 2, \beta: 2, E_p: 2$
990506	1.3066	194.00	20, 2000	-1.37, -2.15	283	$z: 14, S: 5, \alpha: 6, \beta: 5, E_p: 5$
990510	1.6187	19.00	40, 700	-1.23, -2.70	163	$z: 15, S: 2, \alpha: 2, \beta: 2, E_p: 2$
990705	0.8424	75.00	40, 700	-1.05, -2.20	189	$z: 16, S: 2, \alpha: 2, \beta: 2, E_p: 2$
990712	0.4331	11.00	2, 700	-1.88, -2.48	65	$z: 15, S: 17, \alpha: 2, \beta: 2, E_p: 2$
991208	0.7055	100.00	25, 1000	... ,	$z: 18, S: 19$
991216	1.0200	194.00	20, 2000	-1.23, -2.18	318	$z: 20, S: 5, \alpha: 6, \beta: 5, E_p: 5$
000131	4.5000	35.10	26, 1800	-1.20, -2.40	163	$z: 21, S: 21, \alpha: 21, \beta: 21, E_p: 21$
000210	0.8463	61.00	40, 700	... ,	$z: 22, S: 22$
000214	0.4200	1.42	40, 700	-1.62, -2.10	> 82	$z: 23, S: 2, \alpha: 2, \beta: 2, E_p: 2$
000301c	2.0335	2.00	150, 1000	... ,	$z: 24, S: 25,$
000418	1.1182	20.00	15, 1000	... ,	$z: 14, S: 26$
000911	1.0585	230.00	15, 8000	-1.11, -2.32	579	$z: 27, S: 27, \alpha: 27, \beta: 27, E_p: 27$
000926	2.0369	6.20	25, 100	... ,	$z: 28, S: 29$
010222	1.4769	120.00	2, 700	-1.35, -1.64	> 358	$z: 30, S: 31, \alpha: 2, \beta: 2, E_p: 2$
010921	0.4509	18.42	2, 400	-1.55, -2.30	89	$z: 32, S: 33, \alpha: 33, \beta: 34, E_p: 33$
011121	0.3620	24.00	25, 100	-1.42, -2.30 *	217	$z: 35, S: 36, \alpha: 6, E_p: 6$
011211	2.1400	5.00	40, 700	-0.84, -2.30 *	59	$z: 37, S: 37, \alpha: 6, E_p: 6$
020124	3.1980	8.10	2, 400	-0.79, -2.30	120	$z: 38, S: 33, \alpha: 33, \beta: 34, E_p: 33$
020405	0.6899	74.00	15, 2000	0.00, -1.87	192	$z: 39, S: 39, \alpha: 39, \beta: 39, E_p: 40$
020813	1.2550	102.00	30, 400	-1.05, -2.30	212	$z: 41, S: 42, \alpha: 42, \beta: 42, E_p: 42$
021004	2.3351	2.55	2, 400	-1.01, -2.30 *	80	$z: 43, S: 33, \alpha: 33, E_p: 33$
021211	1.0060	3.53	2, 400	-0.80, -2.37	47	$z: 44, S: 45, \alpha: 45, \beta: 45, E_p: 45$
030226	1.9860	5.61	2, 400	-0.89, -2.30	97	$z: 46, S: 45, \alpha: 45, \beta: 34, E_p: 45$
030323	3.3718	1.23	2, 400	-1.62, -2.30 *	...	$z: 47, S: 33, \alpha: 33$
030328	1.5200	36.95	2, 400	-1.14, -2.09	126	$z: 48, S: 33, \alpha: 33, \beta: 33, E_p: 33$
030329	0.1685	110.00	30, 400	-1.26, -2.28	68	$z: 49, S: 50, \alpha: 50, \beta: 50, E_p: 50$
031203	0.1055	1.20	20, 2000	-1.00 *, -2.30 *	> 190	$z: 51, S: 52, E_p: 53$

Table 1—Continued

GRB ^a	z	S_γ ^b [10^{-6} erg cm $^{-2}$]	Bandpass [keV]	$[\alpha, \beta]$ ^c	E_p^{obs} ^d [keV]	References ($z, S_\gamma = S, t_{\text{jet}} = t, n, \alpha, \beta, E_p$)
040924	0.8590	2.73	20, 500	-1.17, -2.30 *	67	$z: 54, S: 55, \alpha: 56, E_p: 55$
041006	0.7160	19.90	25, 100	-1.37, -2.30 *	63	$z: 57, S: 58, \alpha: 56, E_p: 56$
050408	1.2357	1.90	30, 400	-1.98, -2.30 *	20	$z: 59, S: 59, \alpha: 60, E_p: 60$
050525a	0.6060	20.00	15, 350	-1.00, -2.30 *	79	$z: 61, S: 61, \alpha: 61, E_p: 61$
050603	2.2810	34.10	20, 3000	-0.79, -2.15	349	$z: 62, S: 63, \alpha: 63, \beta: 63, E_p: 63$

^aUpper/lower limit data are indicated with $<$ and $>$ respectively. References are given in order for redshift (“ z ”), fluence (“ S ”), low energy band spectral slope (“ α ”), high energy band spectral slope (“ β ”), and spectral peak energy (“ E_p ”).

^bGRB fluence S_γ calculated in the observed bandpass $[e_1, e_2]$ keV.

^c Low energy “Band” spectral slope α and high energy “Band” spectral slope β . When β is reported in the literature but α is not, we set $\alpha = -1.00$ (marked with *). Following Atteia (2003), when α is reported in the literature and β is not, we fix $\beta = -2.30$ (marked with *). When both α and β are not reported in the literature we assume $\alpha = -1.00$ and $\beta = -2.30$.

^dObserved spectral peak energy $E_p^{\text{obs}} = E_p^{\text{obs}}(2 + \alpha)$. When E_p^{obs} is not reported we fix $E_p^{\text{obs}} = 250$ keV. When E_p^{obs} is reported only with a limit, we adopt E_p^{obs} as the value of the limit.

References. — 1. Bloom et al. 2001a; 2. Amati et al. 2002; 3. Bloom et al. 1998; 4. Djorgovski et al. 2001; 5. Jimenez et al. 2001; 6. Amati 2004; 7. Kulkarni et al. 1998; 8. Bloom et al. 1999; 9. Groot et al. 1998; 10. Tinney et al. 1998; 11. Djorgovski et al. 2003; 12. Djorgovski et al. 1998; 13. Kulkarni et al. 1999; 14. Bloom et al. 2003; 15. Vreeswijk et al. 2001; 16. Le Floc’h et al. 2002; 17. Frontera et al. 2001; 18. Djorgovski et al. 1999a; 19. Hurley et al. 2000; 20. Vreeswijk et al. 1999; Djorgovski et al. 1999b; 21. Andersen et al. 2000; 22. Piro et al. 2002; 23. Antonelli et al. 2000; 24. Castro et al. 2000a; 25. Jensen et al. 2001; 26. Berger et al. 2001; 27. Price et al. 2002c; 28. Castro et al. 2000b; 29. Price et al. 2001; 30. Mirabal et al. 2002; 31. in’t Zand et al. 2001; 32. Price et al. 2002a; 33. Sakamoto et al. 2004; 34. Atteia 2003; 35. Garnavich et al. 2003; 36. Price et al. 2002b; 37. Holland et al. 2002; 38. Hjorth et al. 2003; 39. Price et al. 2003a; 40. Price et al. 2003b; 41. Barth et al. 2003; 42. Barraud et al. 2003; 43. Möller et al. 2002; 44. Vreeswijk et al. 2003; 45. Crew et al. 2003; 46. Greiner et al. 2003; 47. Vreeswijk et al. 2004; 48. Martini et al. 2003; 49. Bloom et al. 2003d; 50. Vanderspek 2004a; 51. Prochaska et al. 2003; 52. Watson et al. 2004; 53. Sazonov et al. 2004; 54. Wiersema et al. 2004; 55. Golenetskii et al. 2004; 56. Vanderspek 2004b; 57. Price et al. 2004; 58. Galassi et al. 2004; 59. Berger et al. 2005; 60. Sakamoto et al. 2005; 61. Cummings et al. 2005; 62. Berger et al. 2005; 63. Golenetskii et al. 2005.

- Covino, S., et al. 1999, *A&A*, 348, L1
- Crew, G. B., et al. 2003, *ApJ*, 599, 387
- Cui, X. H., Liang, E. W., & Lu, R. J. 2005, *AJ*, in press (astro-ph/0504372)
- Cummings, J., Barbier, L., & Barthelmy, S. et al. 2005, GCN Report 3479
- Dai, Z. G., & Cheng, K. S. 2001, *ApJ*, 558, L109
- Dai, Z. G., & Gou, L. J. 2001, *ApJ*, 552, 72
- Dai, X. Y., & Zhang, B. 2005, *ApJ*, 621, 875
- Djorgovski, S. G., Bloom, J. S., & Kulkarni, S. R. 2003, *ApJ*, 591, L13
- Djorgovski, S. G., Dierks, A., Bloom, J. S., Kulkarni, S. R., Filippenko, A. V., Hillenbrand, L. A., & Carpenter, J. 1999a, GCN Report 481
- Djorgovski, S. G., Frail, D. A., Kulkarni, S. R., Bloom, J. S., Odewahn, S. C., & Diercks, A. 2001, *ApJ*, 562, 654
- Djorgovski, S. G., Goodrich, R., Kulkarni, S. R., Bloom, J. S., Dierks, A., Harrison, F., & Frail, D. A. 1999b, GCN Report 510
- Djorgovski, S. G., Kulkarni, S. R., Bloom, J. S., Goodrich, R., Frail, D. A., Piro, L., & Palazzi, E. 1998, *ApJ*, 508, L17
- Firmani, C., Avila-Reese, V., Ghisellini, G., et al. 2004, *ApJ*, 611, 1033
- Fox, D. W. et al. 2003, *Nature*, 422, 284
- Frail, D. A. et al. 2001, *ApJ*, 562, L55
- Frontera, F. et al. 2001, *ApJ*, 550, L47
- Galassi, M. et al. 2004, GCN Report 2770
- Garnavich, P. M. et al. 2003, *ApJ*, 582, 924
- Golenetskii, S., Aptekar, R., Mazets, E., Pal'shin, V., Frederiks, D., & Cline, T. 2004, GCN Report 2754
- Golenetskii, S., Aptekar, R., Mazets, E., Pal'shin, V., Frederiks, D., & Cline, T. 2005, GCN Report 3518
- Greiner, J., Guenther, E., Klose, S., & Schwarz, R. 2003, GCN Report 1886
- Groot, P. J. et al. 1998, *ApJ*, 502, L123

- Guetta, D., Piran, T. & Waxman, E. 2005, 619, 412
- Hjorth, J. et al. 2003, ApJ, 597, 699
- Holland, S. T.. 2002, AJ, 124, 639
- Hurley, K. et al. 2000, ApJ, 534, L23
- in’t Zand, J. J. M. et al. 2001, ApJ, 559, 710
- Jensen, B. L. et al. 2001, A&A, 370, 909
- Jimenez, R., Band, D., & Piran, T. 2001, ApJ, 561, 171
- Kulkarni, S. R. et al. 1999, Nature, 398, 389
- Kulkarni, S. R. et al. 1998, Nature, 393, 35
- Lamb, D. Q. 1999, A&A, 138, 607
- Lamb, D. Q., Donaghy, T. Q., & Graziani, C. 2005, ApJ, 620, 355
- Le Floc’h, E. et al. 2002, ApJ, 581, L81
- Liang, E. W., Wu, X. F. & Dai, Z. G. 2004, MNRAS, 354, 81
- Lin, J. R., Zhang, S. N. & Li, T. P. 2004, ApJ, 605, 819
- Lloyd-Ronning, N. M., Dai, X., & Zhang, B. 2004, ApJ, 601, 371
- Madau, P., & Pozzetti, L. 2000, MNRAS, 312, L9
- Martini, P., Garnavich, P., & Stanek, K. Z. 2003, GCN Report 1980
- Mészáros, P., Ramirez-Ruiz, E., Rees, M. J., & Zhang, B. 2002, ApJ, 578, 812
- Mészáros, P., Rees, M. J., & Wijers, R. A. M. J. 1998, ApJ, 499, 301
- Mirabal, N. et al. 2002, ApJ, 578, 818
- Möller, P. et al. 2002, A&A, 396, L21
- Nakar, E., Granot, J., & Guetta D. 2004, ApJ, 606, L37
- Nakar, E., Piran, T., & Granot, J. 2003, NewA, 8, 495
- Paczynski, B. 1998, ApJ, 494, L45
- Panaitescu, A., & Kumar, P. 2001, ApJ, 560, L49

- Panaiteescu, A., & Kumar, P. 2002, *ApJ*, 571, 779
- Perna, R., Sari, R., & Frail, D. 2003, *ApJ*, 594, 379
- Piro, L. et al. 2002, *ApJ*, 577, 680
- Porciani, C., & Madau, P. 2001, *ApJ*, 548, 522
- Preece, R. D., Briggs, M. S., Pendleton, G. N., Paciesas, W. S., & Band, D. L. 2000, *ApJ*, 126, 19
- Press, W. H., Teukolsky, S. A., Vetterling, B. P., & Flannery, B. P. 1997, *Numerical Recipes*, Cambridge Univ. Press
- Price, P. A. et al. 2001, *ApJ*, 549, L7
- Price, P. A. et al. 2002a, *ApJ*, 573, 85
- Price, P. A. et al. 2002b, *ApJ*, 572, L51
- Price, P. A. et al. 2002c, *ApJ*, 571, L121
- Price, P. A. et al. 2003a, *ApJ*, 589, 838
- Price, P. A. et al. 2003b, *ApJ*, 584, 931
- Price, P. A., Roth, K., Rich, J., Schmidt, B. P., Peterson, B. A., Cowie, L., Smith, C., & Rest, A. 2004, *GCN Report* 2791
- Prochaska, J. X., Bloom, J. S., Chen, H. W., Hurley, K., Dressler, A., & Osip, D. 2003, *GCN Report* 2482
- Ramirez-Ruiz, E., Granot, J., Kouveliotou, C., Woosley, S. E., Patel, S. K., & Mazzali, P. A. 2005, *ApJ*, 625, L91
- Rhoads, J. E. 1997, *ApJ*, 487, L1
- Rossi, E., Lazzati, D., & Rees, M. J. 2002, *New Astronomy*, 7, 197
- Sakamoto, T. et al. 2004, *astro-ph/0409128*
- Sakamoto, T. et al. 2005, *GCN Report* 3189
- Sari, R., Piran, T., & Halpern, J. P. 1999, *ApJ*, 519, L17
- Sazonov, S. Y., Lutovinov, A. A., & Sunyaev, R. A. 2004, *Nature*, 430, 646
- Steidel, C. C., Adelberger, K. L., Giavalisco, M., Dickinson, M., & Pettini, M. 1999, *ApJ*, 519, 1

- Tinney, C., Stathakis, R., Cannon, R., & Galama, T. J. 1998, IAU Circ., 6896, 1
- Vanderspek, R. 2004a, ApJ, 617, 1251
- Vanderspek, R. 2004b, <http://space.mit.edu/HETE/Bursts/Data/>
- Vreeswijk, P., Rol, E., Hjorth, J., et al. 1999, GCN Report 496
- Vreeswijk, P., Fruchter, A., Hjorth, J., & Kouveliotou, C. 2003, GCN Report 1785
- Vreeswijk, P. M. et al. 2001, ApJ, 546, 672
- Vreeswijk, P. M. et al. 2004, A&A, 419, 927
- Watson, D. et al. 2004, ApJ, 605, L101
- Wiersema, K., C, R. L., Rol, E., Vreeswijk, P., & M, R. A. 2004, GCN Report 2800
- Wijers, R. A. M. J., et al. 1999, ApJ, 523, L33
- Woosley, S. 1993, ApJ, 405, 273
- Wu, X. F., Dai, Z. G., & Liang, E. W. 2004, ApJ, 615, 359
- Xu, L., & Dai, Z. G. 2004, Chin. J. Astron. Astrophys., 4, 267
- Yamazaki, R., Yonetoku, D., & Nakamura, T. 2003, ApJ, 594, L79
- Zhang, B., Dai, X. Y., Lloyd-Ronning, & Mészáros, P. 2004, ApJ, 601, L119
- Zhang, B., & Mészáros, P. 2002, ApJ, 571, 876

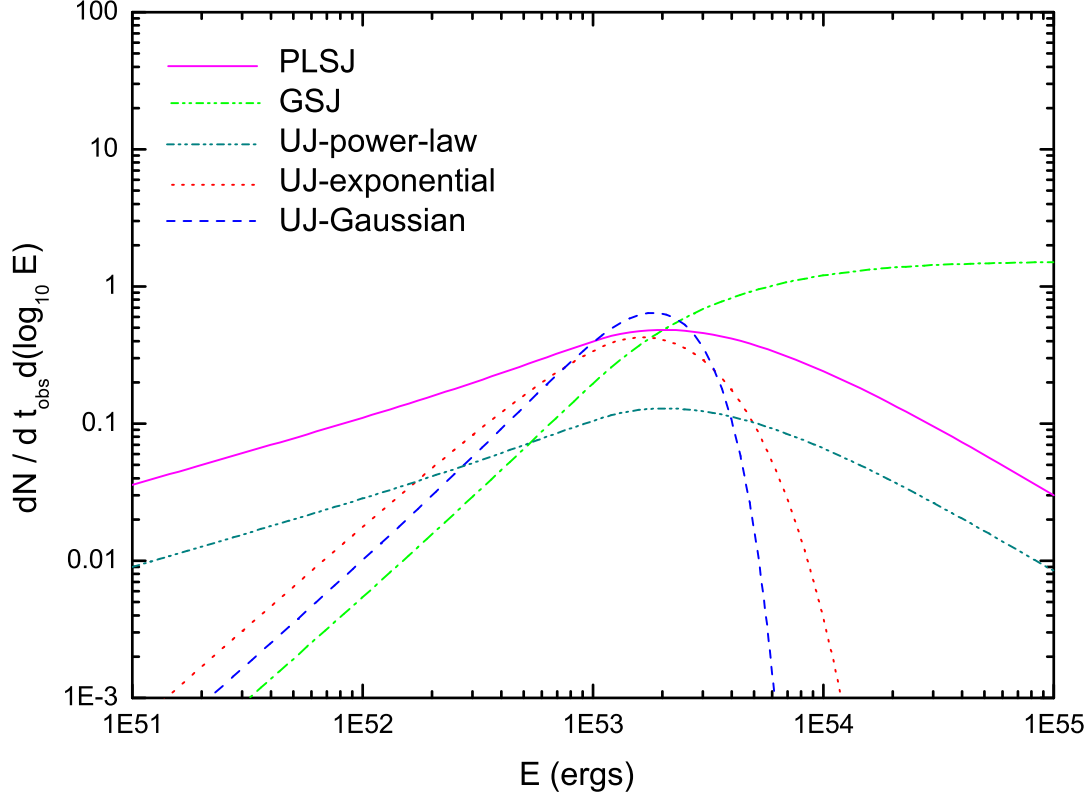


Fig. 1.— The observed differential rate of GRBs as a function of E for 5 kinds of jet model. The parameter T is chosen to be 8 s for all GRBs. Other parameters are assumed: $L = -1$, $E_j = 10^{51}$ ergs, $f_{\text{GRB}} = 10^{-8} M_{\odot}^{-1}$, and $F_{\text{ph,lim}} = 0.424 \text{ photons} \cdot \text{cm}^{-2} \cdot \text{s}^{-1}$. For power-law structured jet models, $k_E = 2.0$ and $\theta_c = 0.01$. For the Gaussian structured jet model, $\theta_c = 0.05$. For the uniform jet model $\lambda = 0.7 \times 10^{-53} \text{ ergs}^{-1}$ (the exponential case); $\zeta = -1.1$ (the power-law case); $\bar{E} = 0.7 \times 10^{53}$ ergs, $\sigma = 1.4 \times 10^{53}$ ergs (the Gaussian case). Here we take the star formation rate model 2 as an example.

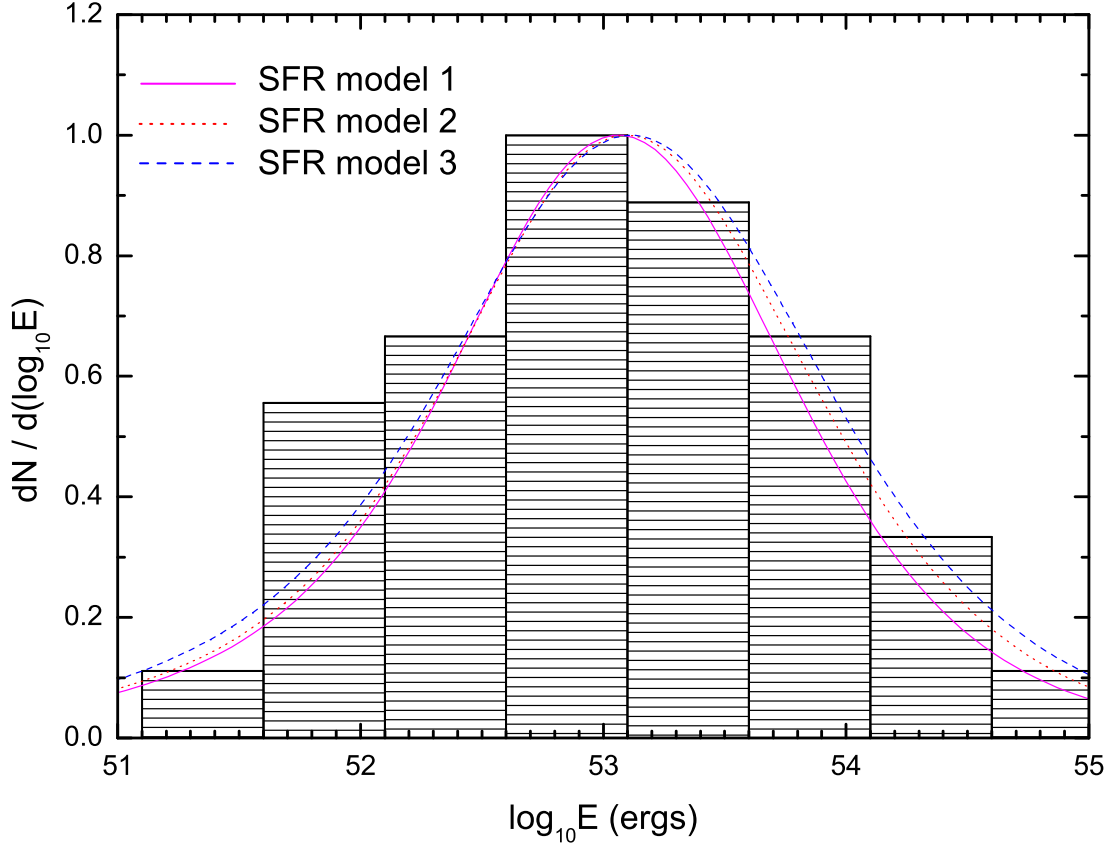


Fig. 2.— Theoretical distribution of the isotropic-equivalent energy in the power-law structured jet model (lines), compared with the observed distribution from a sample of 39 GRBs with known redshifts detected so far (histogram). Different lines correspond to different star formation rate models. The parameters: $k_E = 2.3$ and $\theta_c = 0.02$. Here we take $L = -1$ as an example.

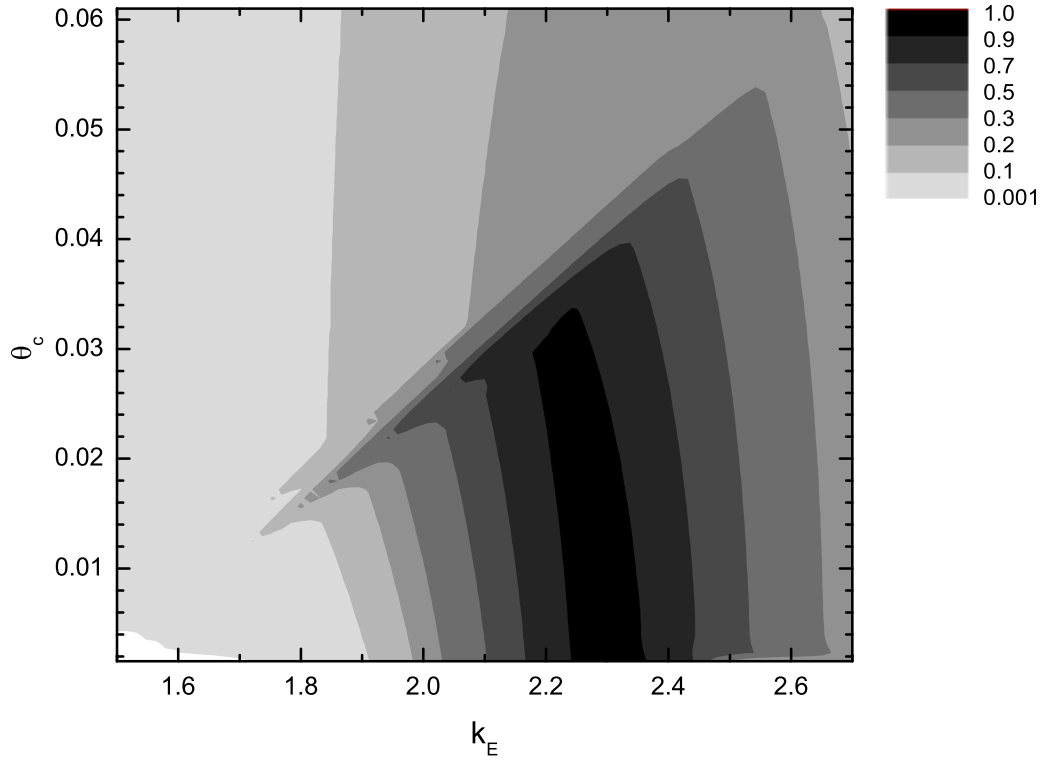


Fig. 3.— The Gray scale map of the K-S test result for different values of k_E and θ_c . Every point in this plot corresponds to a set of parameters for the PLSJ model and the color of the point represents how well the PLSJ model with such parameters is compared with the observed data. Here we take the star formation rate model 2 and $L = -1$ as an example.

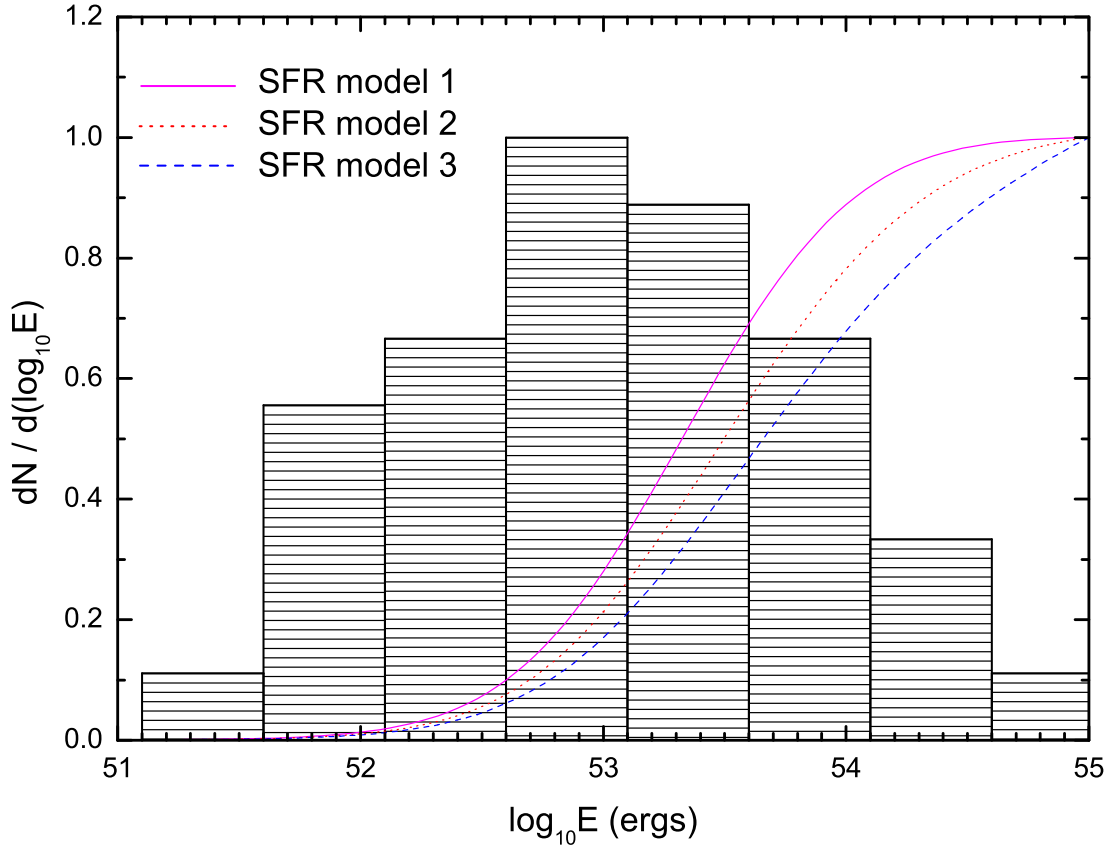


Fig. 4.— Theoretical distribution of the isotropic-equivalent energy in the Gaussian structured jet model (lines), compared with the observed distribution from a sample of 39 GRBs with known fluences and redshifts detected so far (histogram). Different lines correspond to different star formation rate models. The parameter $\theta_c = 0.01$. Here we take $L = -1$ as an example.

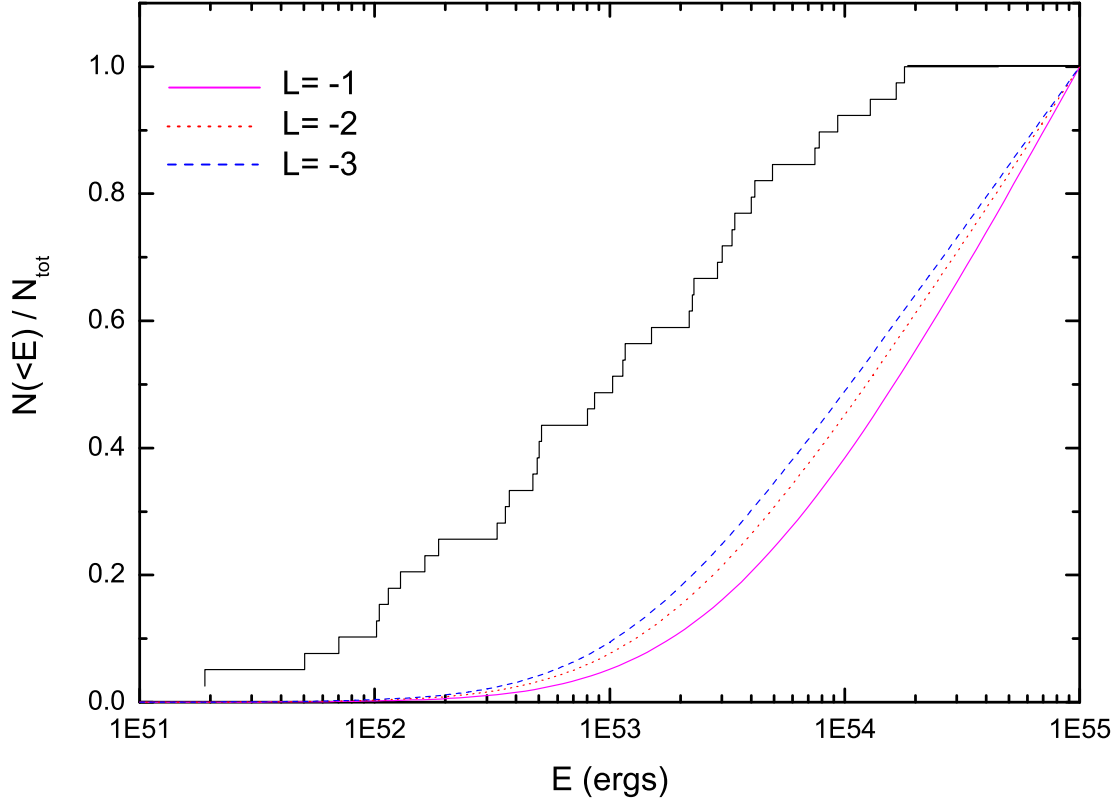


Fig. 5.— Cumulative distribution for the Gaussian structured jet model. Three values of L , the index in the redshift-identification selection effect, are considered. The cumulative histogram is plotted from the sample. The parameter $\theta_c = 0.01$. Here we take star formation rate model 2 as an example.

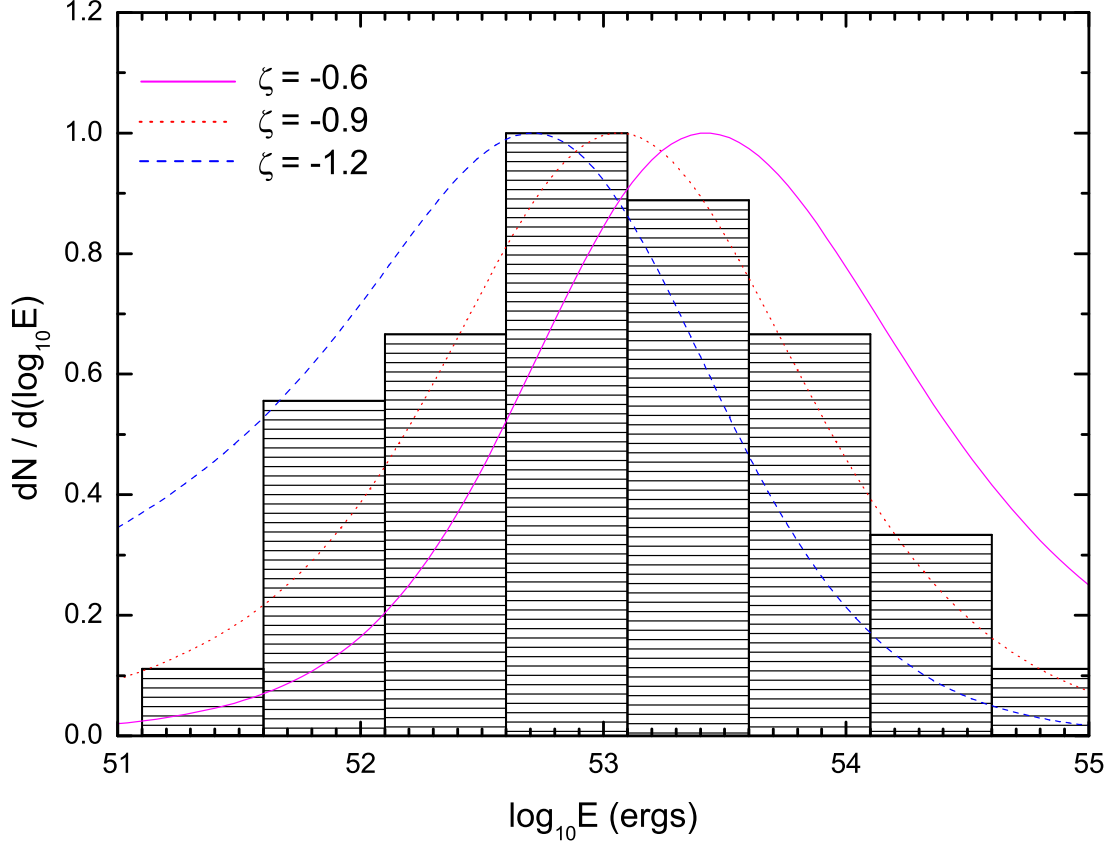


Fig. 6.— Theoretical distribution of the isotropic-equivalent energy in the uniform jet model in the case that the distribution of isotropic-equivalent energy is a power-law function (lines), compared with the observed distribution from a sample of 39 GRBs with known fluences and redshifts detected so far (histogram). Different lines correspond to different values of the power-law index ζ . Here we take the star formation rate model 2 and $L = -1$ as an example.

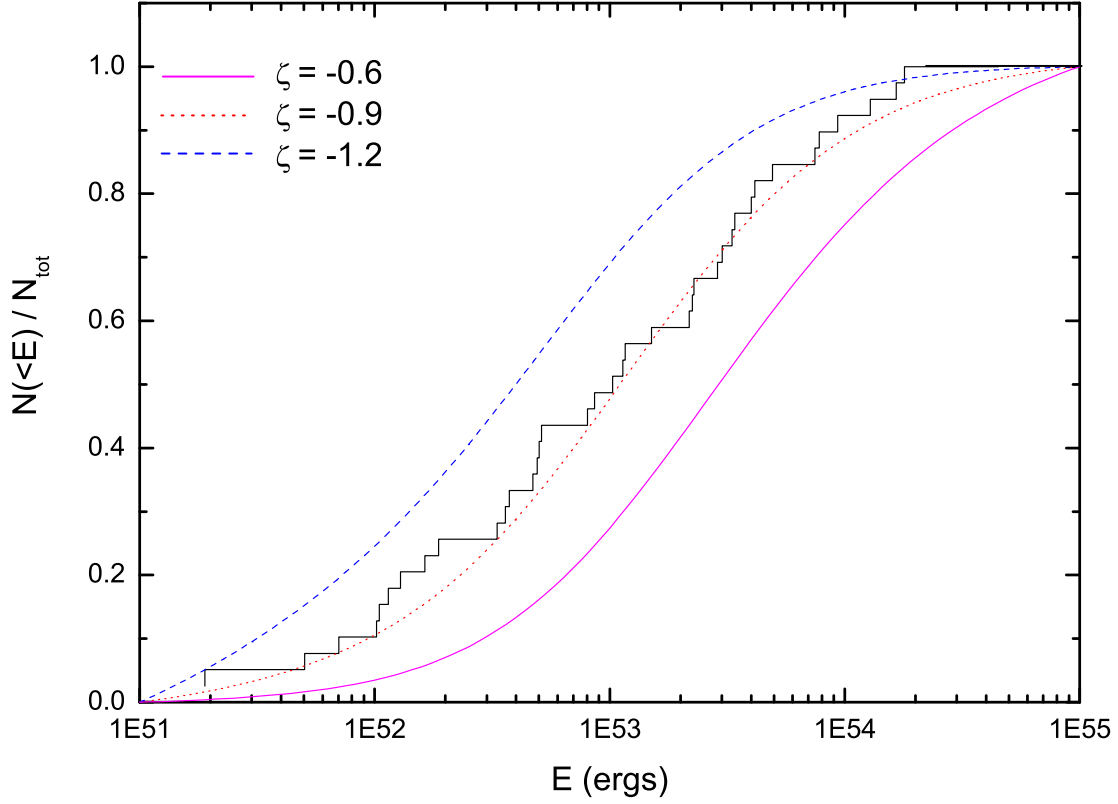


Fig. 7.— Cumulative distribution for the uniform jet model in the case that the distribution of isotropic-equivalent energy is a power-law function. Different lines correspond to the different values of the power-law index ζ . The cumulative histogram is plotted from the sample. Here we take the star formation rate model 2 and $L = -1$ as an example.

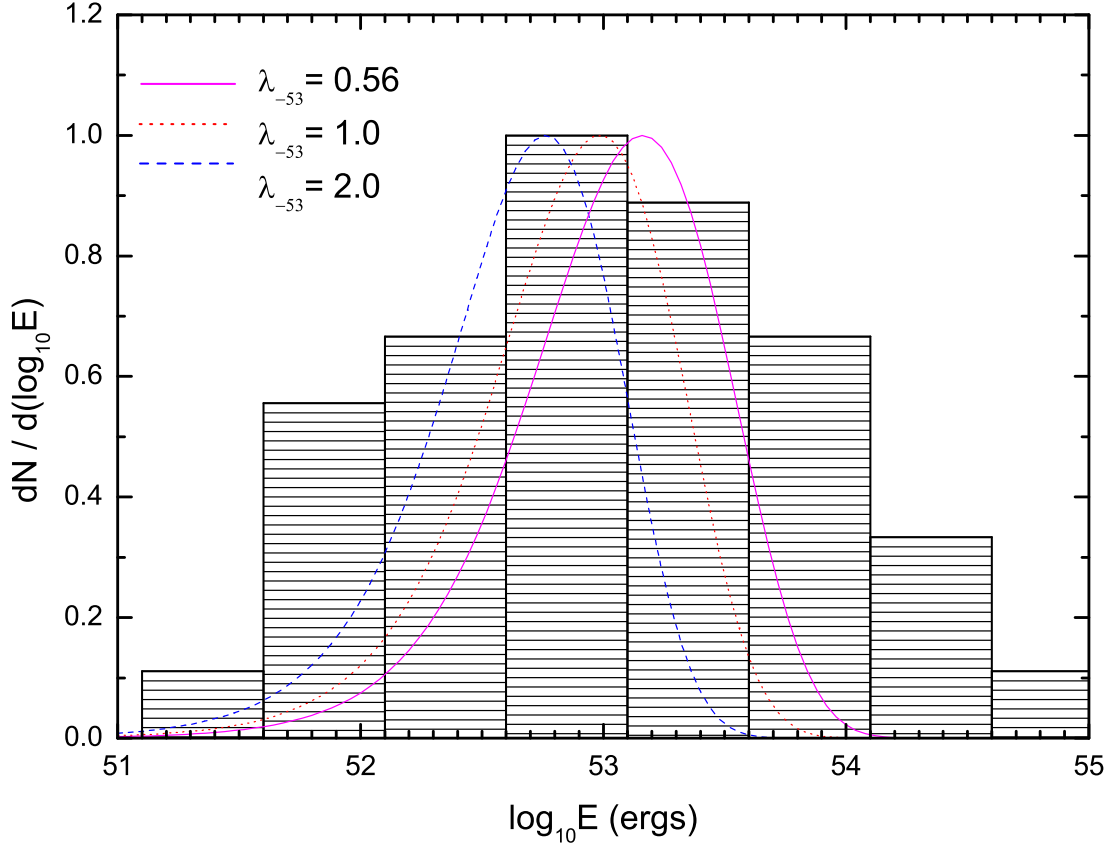


Fig. 8.— Theoretical distribution of the isotropic-equivalent energy in the uniform jet model in the case that the distribution of isotropic-equivalent energy is an exponential function (lines), compared with the observed distribution from a sample of 39 GRBs with known fluences and redshifts detected so far (histogram). Different lines correspond to different values of the exponential parameter λ . Here we take the star formation rate model 2 and $L = -1$ as an example.

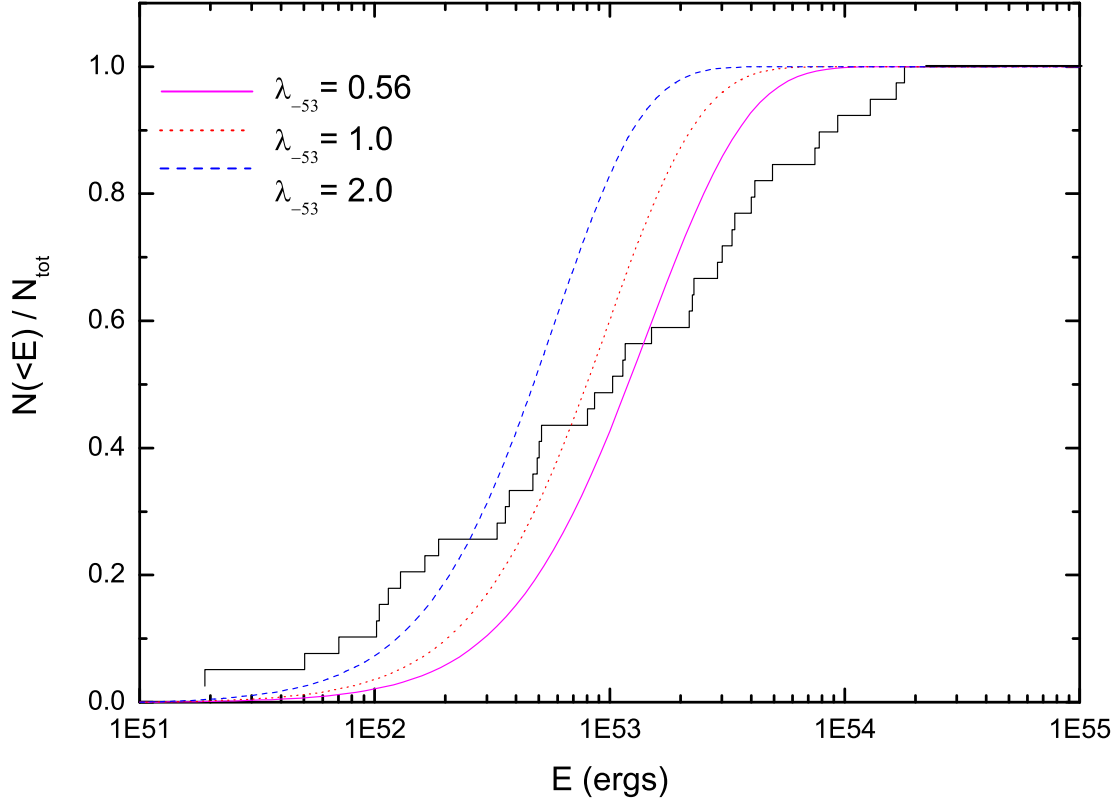


Fig. 9.— Cumulative distribution for the uniform jet model in the case that the distribution of isotropic-equivalent energy is an exponential function. Three values of λ are considered. The cumulative histogram is plotted from the sample. Here we take the star formation rate model 2 and $L = -1$ as an example.

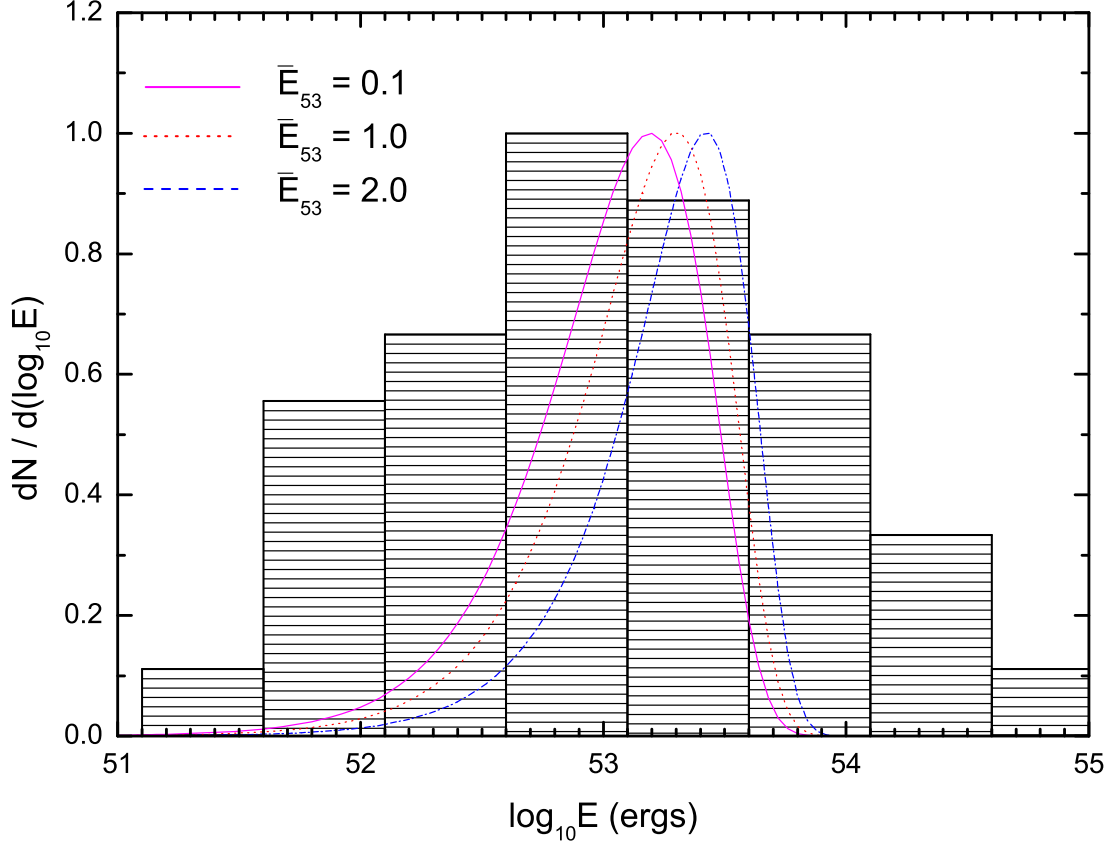


Fig. 10.— Theoretical distribution of the isotropic-equivalent energy in the uniform jet model in the case that the distribution of isotropic-equivalent energy is a Gaussian function (lines), compared with the observed distribution from a sample of 39 GRBs with known fluences and redshifts detected so far (histogram). Different lines correspond to different values of mean energy \bar{E} (in the units of ergs). We adopt the scatter in the Gaussian function as $\sigma = 1.7 \times 10^{53}$ ergs. Here we take the star formation rate model 2 and $L = -1$ as an example.

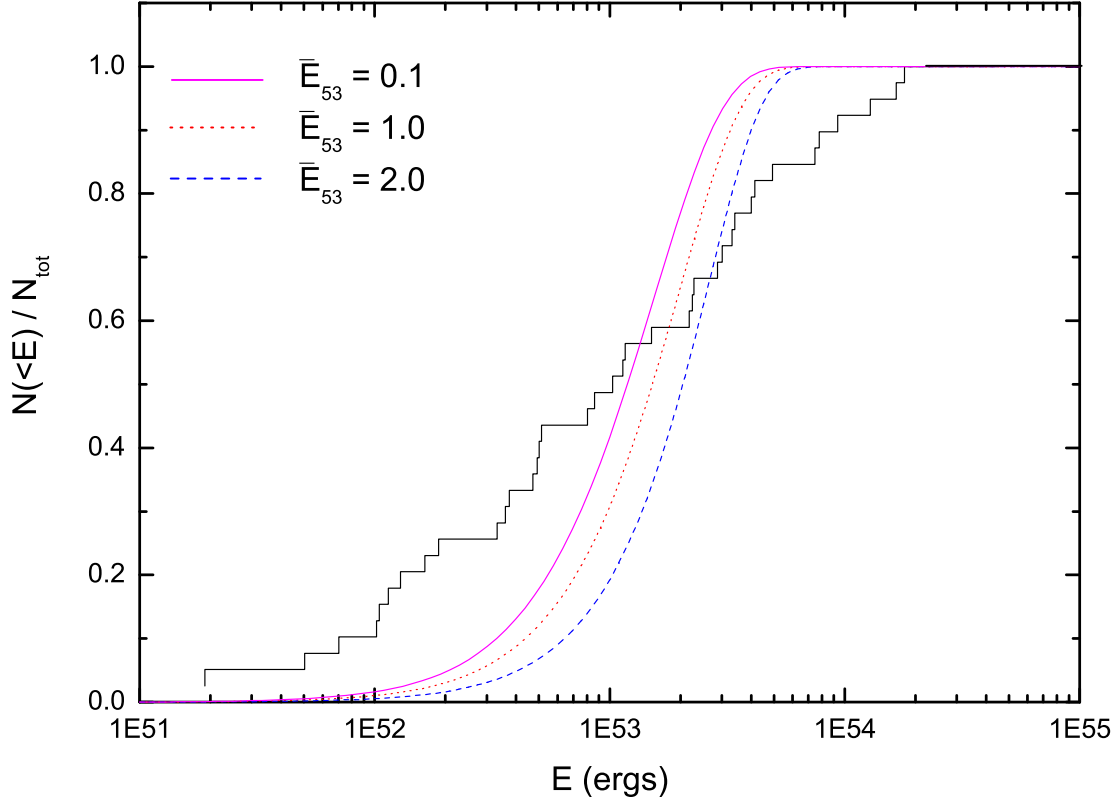


Fig. 11.— Cumulative distribution for the uniform jet model in the case that the distribution of isotropic-equivalent energy is a Gaussian function. Different lines correspond to different values of mean energy \bar{E} (in the units of ergs). We adopt the scatter in the Gaussian function as $\sigma = 1.7 \times 10^{53}$ ergs. The cumulative histogram is plotted from the sample. Here we take the star formation rate model 2 and $L = -1$ as an example.

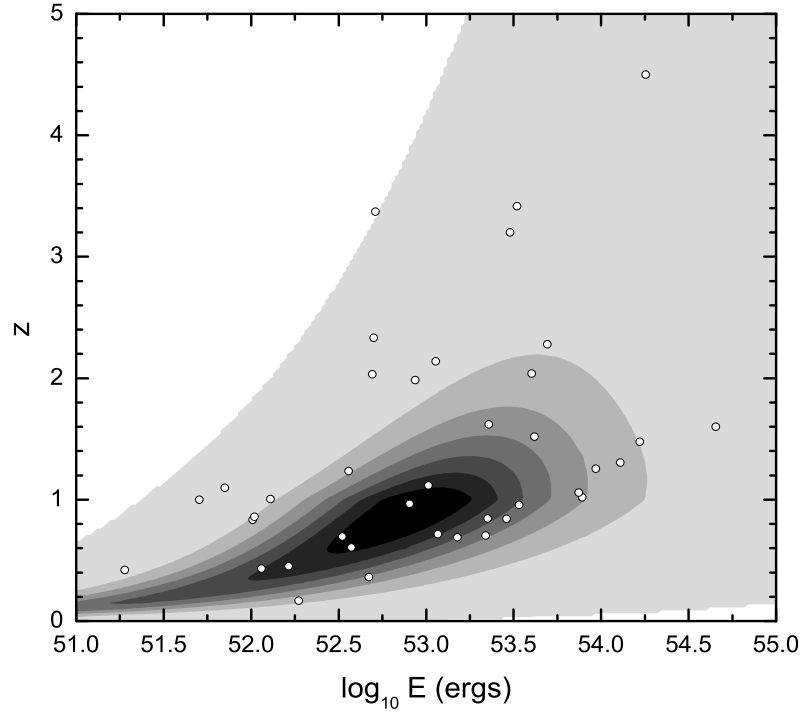


Fig. 12.— The 2D distribution density, $\dot{N}(E, z)$, for the power-law structured jet model and star formation rate model 2. The parameters are assumed: $L = -1$, $k_E = 2.2$, and $\theta_c = 0.02$. The circles denote 39 bursts with known fluences and redshifts detected so far.

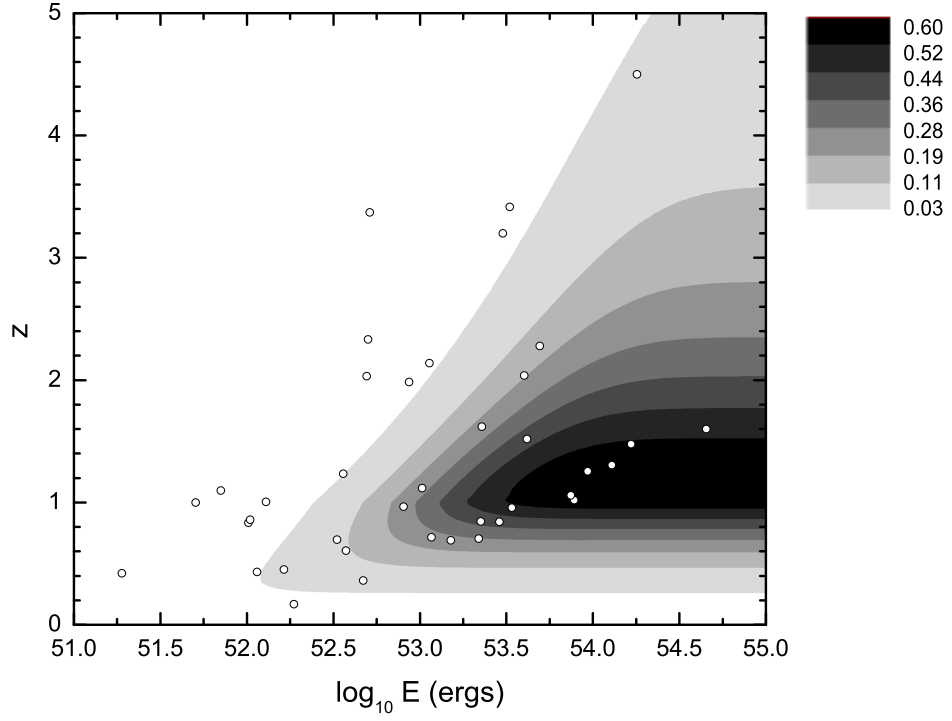


Fig. 13.— The 2D distribution density, $\dot{N}(E, z)$, for the Gaussian structured jet model, star formation rate model 2. The parameters are assumed: $L = -1$ and $\theta_c = 0.05$. The circles denote 39 bursts with known fluences and redshifts detected so far.

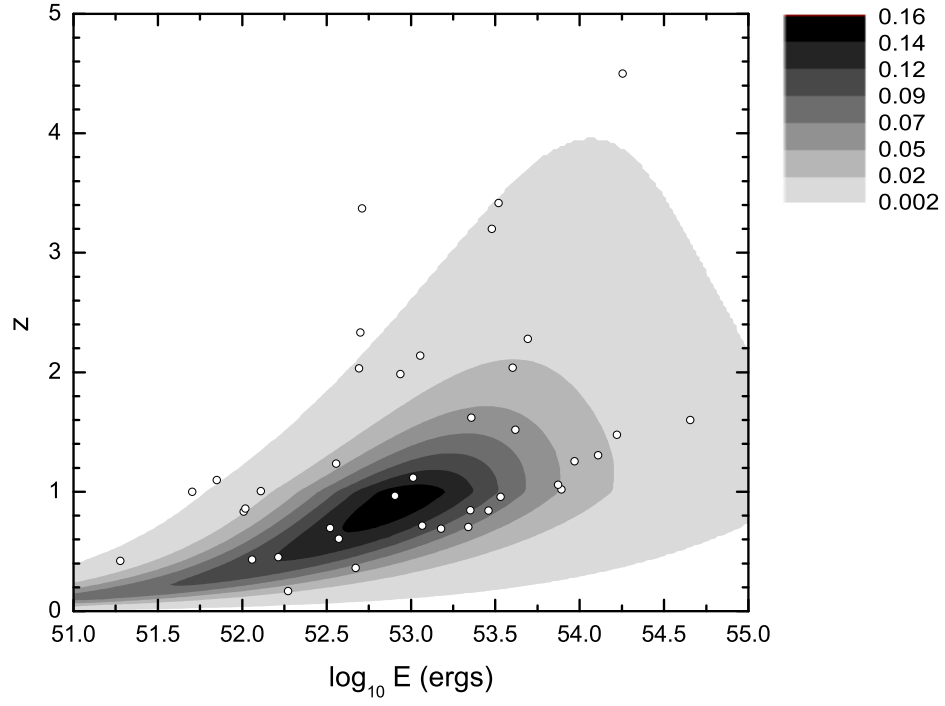


Fig. 14.— The 2D distribution density, $\dot{N}(E, z)$, for the uniform jet model (the power-law case) and star formation rate model 2. The parameters are assumed: $L = -1$ and $\zeta = -0.9$. The circles denote 39 bursts with known fluences and redshifts detected so far.

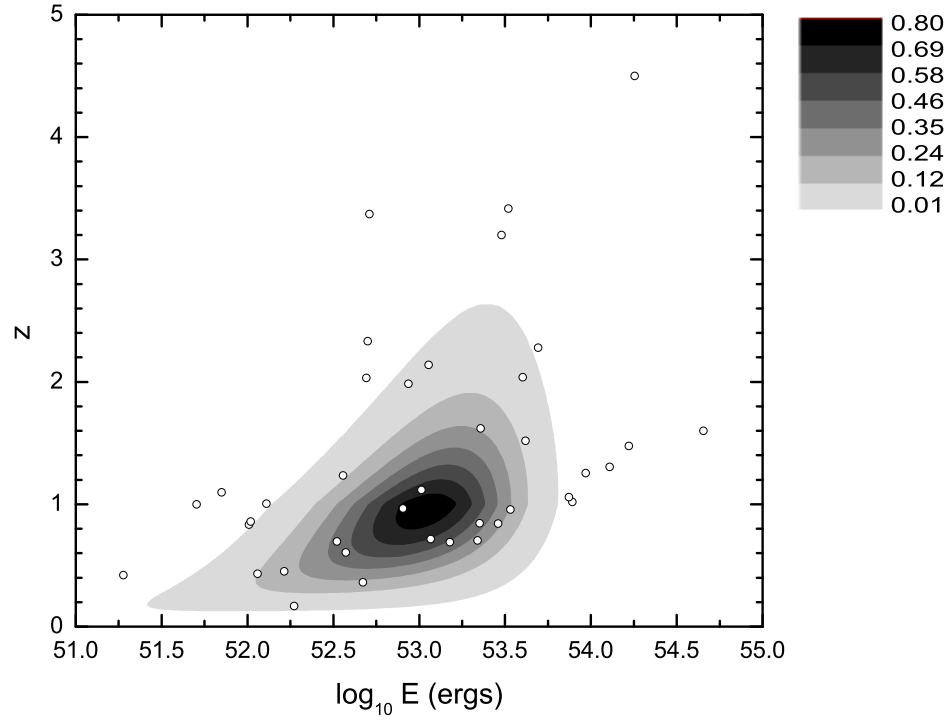


Fig. 15.— The 2D distribution density, $\dot{N}(E, z)$, for the uniform jet model (the exponential case) and star formation rate model 2. The parameters are assumed: $L = -1$ and $\lambda = 0.7 \times 10^{-53} \text{ ergs}^{-1}$. The circles denote 39 bursts with known fluences and redshifts detected so far.

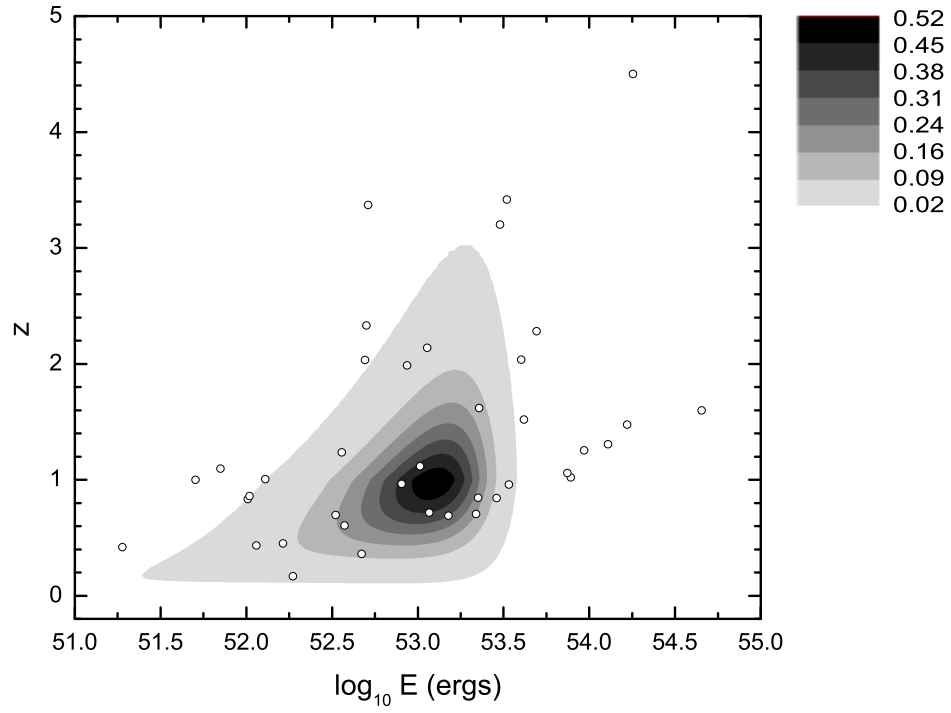


Fig. 16.— The 2D distribution density, $\dot{N}(E, z)$, for the uniform jet model (the Gaussian case) and star formation rate model 2. The parameters are assumed: $L = -1$ and $\bar{E} = 0.7 \times 10^{53}$ ergs, and $\sigma = 1.0 \times 10^{53}$ ergs. The circles denote 39 bursts with known fluences and redshifts detected so far.